CNN-Based Pressure Prediction for a Hybrid Pneumatic–Electromagnetic Bonding System in the OLED Lamination Process

Taehun Ju[1,2], Hohyun Lee[3], Eun-Ho Lee[3,4,5†]
[1]Department of Semiconductor and Display Engineering, Sungkyunkwan University, Suwon 16419, Korea
[2]Samsung Institute of Technology, Yongin 17113, Korea
[3]Mechanical Engineering, San José State University, San Jose, CA 95192, USA
[4]Department of Mechanical Engineering, Sungkyunkwan University, Suwon 16419, Korea,
[5]Department of Intelligent Robotics, Sungkyunkwan University, Suwon 16419, Korea
Ph: +82-10-3228-0182
Email: e.h.lee@skku.edu

Abstract

As OLED adoption for large displays continues to grow, there is a need for compact equipment designs that can apply uniform pressure during display and cover glass adhesion. In this study, we propose a multiphysics design methodology using electromagnetic and pneumatic actuators, which offers advantage in terms of actuator size and fast responsiveness. Through experiments, we confirmed that this system improves pressure uniformity by up to 53.7%p. Furthermore, we built a CNN-based image generation model that can help us predict the pressure distribution during the process without high-cost experiments or time-consuming simulations. We first compared the experimental data with the FEM simulation and found that the error is approximately 4.6%. After that, we confirmed that there is an error of less than 6% between the simulation and the CNN model's predictions.

Key words

OLED, Simulation, CNN, Multi-physics, Pressure-Prediction

I. Introduction

The adoption of polyimide for OLED backplane substrates has enabled a variety of form factors in smartphones, such as foldable and rollable displays, due to its flexibility. As the display market transitions from LCD to OLED, larger LCD displays used for TVs, tablets, and automotive applications are also being replaced with OLED. Thanks to these flexible characteristics, the display shape is not restricted to a simple flat rectangle. However, attaching cover windows and optically clear adhesives (OCAs)—a process called lamination to minimize light loss and reflection outdoors—is still essential [1]–[3], and attaching them onto large 3D flexible displays, such as curved ones, is getting more difficult. Just adding actuators without deliberation regarding compact design can cause higher costs and bigger equipment, which consequently lowers factory floor efficiency. The proposed configuration in this study involves a pneumatic actuator and an electromagnetic actuator to solve this twofold problem: compact size and uniform pressure application on large displays.

Fig. 1 shows the most common designs for attaching cover glasses and OCAs. The first one uses a soft roller, and the second one uses a flat electrostatic chuck (ESC), which guarantees better quality because it can prevent substrates from pressure concentration during the bonding process.

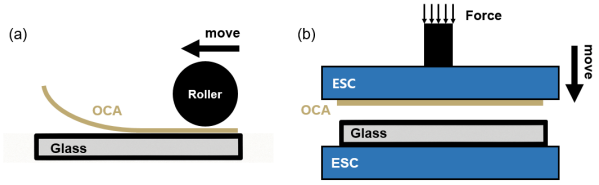


Figure 1 (a) Roll Lamination (b) Flat Lamination

In industrial lamination equipment, a pneumatic actuator is located in the middle of the system to apply force, and a shaft transfers the input force to the substrates. When the substrate size is small, like 6–7 inch smartphones, this method is sufficiently capable of suppressing edge defects such as bubbles and delamination. However, as shown in Fig. 2, the pressure deviation between the center and the edge results in defects during the large-display lamination process. Although adopting more actuators looks like a simple solution, the number of actuators determines the equipment

size and cost. Therefore, we devised a novel hardware configuration not only to miniaturize the system but also to suppress defects at the edges during the process.

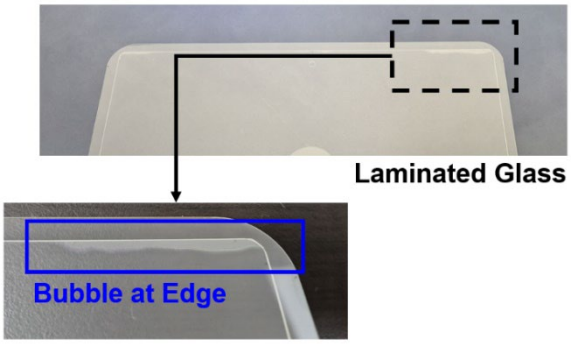


Figure 2 Edge Bubble in Laminated Glass

Fig. 3 shows the laboratory lamination equipment involving the electromagnetic (EM) actuator, which consists of a metallic core, case, bobbin, and solenoid. The experiment was performed using a pressure measurement film (Prescale, Fujifilm, Japan) that changes color in proportion to the applied pressure.

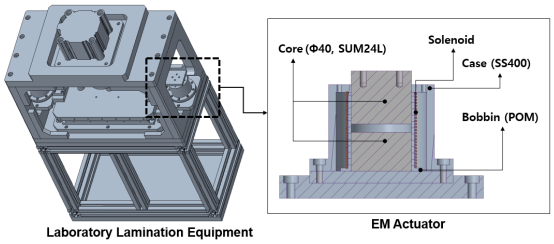


Figure 3 Laboratory Lamination Equipment with EM Actuator

II. Experiments

Fig. 4 shows the overall system design used to control the experiment. The main pressure was regulated through an electro-pneumatic regulator using serial communication (RS-232C), and the auxiliary pressure was applied at the system edge to minimize the pressure deviation. The current flowing through the solenoid was adjusted manually in the electric circuit, as shown in Fig. 5.

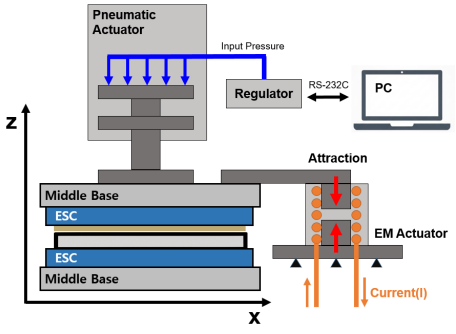


Figure 4 Equipment System Design

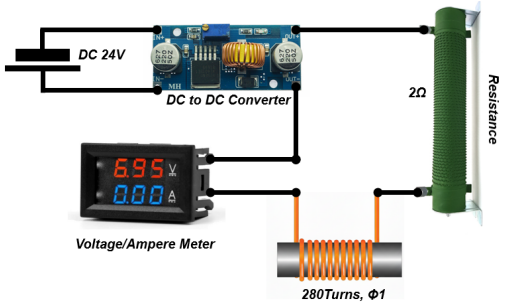


Figure 5 Electric Circuit for EM Actuator

Pressure measurement films were cut into a long strip and positioned to measure both the center and the periphery simultaneously, as indicated by the dashed lines in Fig. 6.

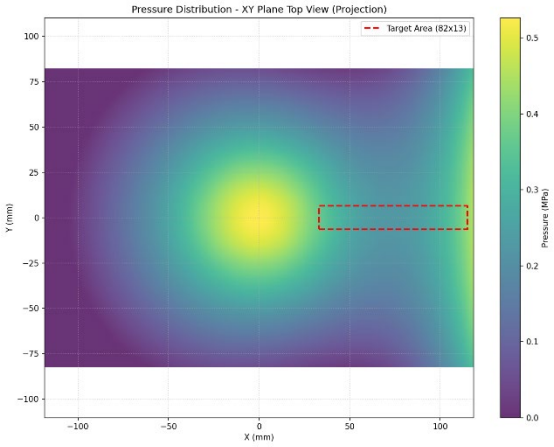


Figure 6 Pressure Measurement Position

III. Theoretical Background

symbols	Description
$\boldsymbol{v}$	Velocity Vector
ϵ_0	Vacuum permittivity
μ_0	Vacuum permeability
$\boldsymbol{e}$	Electric field intensity
$\boldsymbol{h}$	Magnetic field intensity
$\boldsymbol{t}$	Traction vector
$\boldsymbol{t_{EM}}$	Electromagnetic surface force vector
$\boldsymbol{T}$	Cauchy stress tensor
$\boldsymbol{T_{EM}}$	Maxwell stress tensor
$\mathbf{n}$	Unit normal vector pointing outward from the surface
ρ	Density

$\boldsymbol{b}$	Mechanical body force vector

The lamination system follows the first law of thermodynamics, where the applied energy in the form of external force is converted into physical bonding between the OCAs and substrates via Van der Waals forces. Because the external force involves both pneumatic and electromagnetic forces, we introduce thermodynamic balance laws to explain the electromagnetic and mechanical energy conversion in the system, inspired by [6]–[8], as follows.

$$\dot{E} = \dot{H} + \dot{S} \tag{1}$$

$$\dot{E} = \frac{d}{dt}\int_V \left[\rho\left(\epsilon + \frac{1}{2}\boldsymbol{v}\cdot\boldsymbol{v}\right) + \frac{1}{2}(\epsilon_0 \boldsymbol{e}\cdot\boldsymbol{e} + \mu_0 \boldsymbol{h}\cdot\boldsymbol{h})\right] dV \tag{2}$$

$$\dot{H} = \int_{\partial V} \{(\boldsymbol{t} + \boldsymbol{t_{EM}})\cdot\boldsymbol{v} - (\boldsymbol{e}\times\boldsymbol{h})\cdot\boldsymbol{n}\} dA \tag{3}$$

$$\dot{S} = \int_V \rho\, \boldsymbol{b}\cdot\boldsymbol{v} dV \tag{4}$$

$$\boldsymbol{t} = \boldsymbol{T}\cdot\boldsymbol{n} \tag{5}$$

$$\boldsymbol{t_{EM}} = \boldsymbol{T_{EM}}\cdot\boldsymbol{n} \tag{6}$$

Equation (1) shows the global thermodynamic energy balance equation. Substituting the related terms in Equations (2)–(6) results in (7), where the corresponding terms can be classified according to their physical meanings into (8)–(10), which represent the continuity equation, the balance of momentum equation, and the balance of energy equation, respectively.

$$\dot{\rho}\left(\epsilon + \tfrac{1}{2}v\cdot v\right) + \rho(\dot{\epsilon} + v\cdot\dot{v}) + \rho\left(\epsilon + \tfrac{1}{2}v\cdot v\right)\nabla\cdot v + \epsilon_0 e\cdot \dot{e} + \mu_0 h\cdot\dot{h} + \tfrac{1}{2}(\epsilon_0 e\cdot e + \mu_0 h\cdot h)\nabla\cdot v = v\cdot\left(\nabla\cdot(T + T_{EM})\right) + (T + T_{EM}):\nabla v - \nabla\cdot(e\times h) + \rho b\cdot v \tag{7}$$

$$(\dot{\rho} + \rho\nabla\cdot v)\left(\epsilon + \frac{1}{2}v\cdot v\right) = 0 \tag{8}$$

$$\rho\boldsymbol{v}\cdot\dot{\boldsymbol{v}} = \boldsymbol{v}\cdot\left(\nabla\cdot(\boldsymbol{T} + \boldsymbol{T_{EM}})\right) + \rho\boldsymbol{b}\cdot\boldsymbol{v} \tag{9}$$

$$\rho\dot{\epsilon} = (T + T_{EM}):\nabla v - \nabla\cdot(e\times h) - \left\{\epsilon_0 e\cdot\dot{e} + \mu_0 h\cdot\dot{h} + \tfrac{1}{2}(\epsilon_0 e\cdot e + \mu_0 h\cdot h)\nabla\cdot v\right\} \tag{10}$$

The governing equations related to the EM actuator are (15)–(18), which represent Maxwell's equations.

$$\nabla\cdot D = \rho_f \tag{15}$$

$$\nabla\cdot B = 0 \tag{16}$$

$$\nabla\times E = -\frac{\partial B}{\partial t} \tag{17}$$

$$\nabla\times H = J + \frac{\partial D}{\partial t} \tag{18}$$

IV. Results

Figure 8 shows the experimental results, where the deviation in magenta color depth decreases in proportion to the applied current, meaning that the applied pressure deviation was gradually improved. The main force was set to 4400 N to achieve the target pressure of 0.1–0.2 MPa, which is appropriate for OCA lamination [1]. The pressurized area was a 236 mm × 164 mm glass plate, chosen to imitate 11-inch tablet cover glass OCA lamination. These sheets were scanned and converted into grayscale images to compare the color depth using single values, and the average gray values of the regions of interest were calculated, as shown in Fig. 9. The images were filtered to remove salt-and-pepper noise. After that, the grayscale values inside the blue rectangle were calculated and compared. To determine this index, a weighted average was calculated using a weighting factor of 0.299:0.587:0.114 [4], [5].

Table 1 shows the grayscale deviation ratio (α) between the center and the edge. Although the deviation ratio was 61.7% without the application of electromagnetic force, it significantly improved to 7.98% when an auxiliary force was applied with a 5 A current.

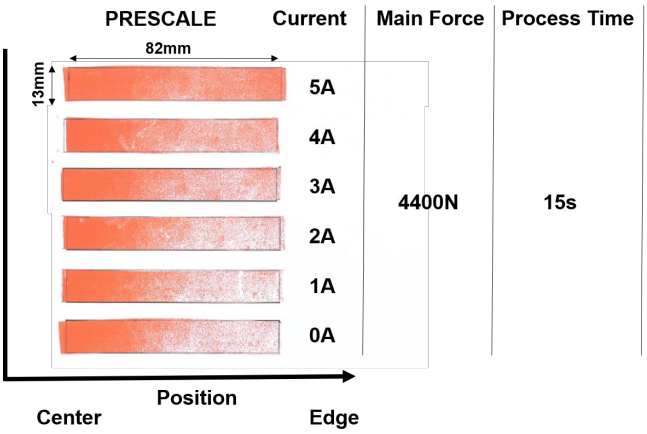


Figure 8 Pressure Measurement Experiment



Figure 9 (a) Grayscale conversion.
(b) Median Filter Applied

	Current					
	N/A	1A	2A	3A	4A	5A
Center	153.02	152.53	151.83	152.57	151.47	155.37
Edge	247.43	244.17	238.18	212.44	200.5	167.77
Δ	94.41	91.64	86.35	59.87	49.03	12.4
α(%)	61.70%	60.08%	56.87%	39.24%	32.37%	7.98%

Table 1. Grayscale and α Value of Median Filtered Image

V. Simulation and CNN Model for Pressure Prediction

Fig. 10 shows the FEM simulation results used to predict the generated electromagnetic force and applied pressure in the designed lamination equipment equipped with the EM actuator. The maximum magnetic flux density of 2.12 T forms around the air gap between the core materials, which is transmitted to the system edge to pressurize it, thereby improving the pressure deviation between the center and the edge, as proven in the experiments.

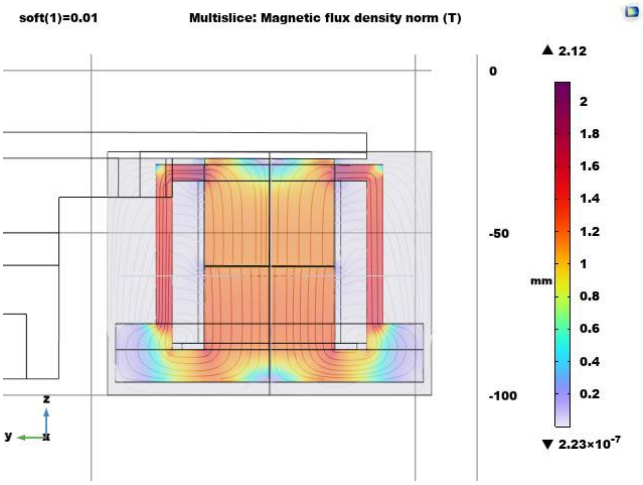


Figure 10 Electromagnetic Actuator FEM Simulation

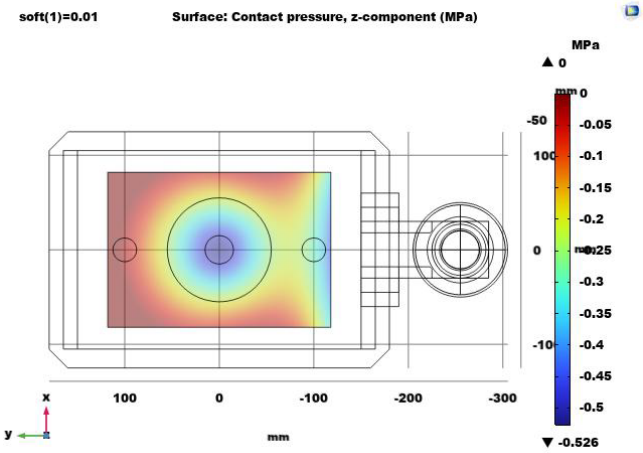


Figure 11 Contact Pressure Simulation

The pressure data at the nodes were converted into grayscale values to compare them with the experimental data using a calibration curve, which indicates the pressure versus grayscale value relationship conducted separately, as shown in Fig. 12. Pressures from 0.1 to 0.8 MPa were applied to the pressure measurement films, which were then scanned and converted into grayscale values to fit the calibration curve.

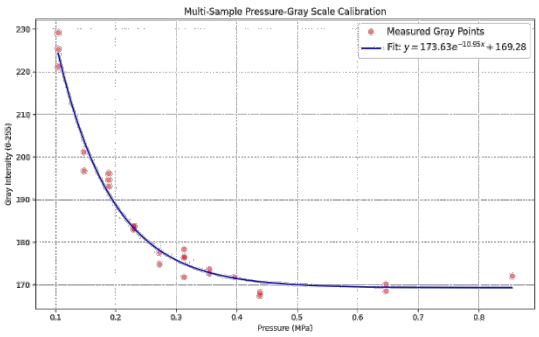


Figure 12 Pressure vs Grayscale Value Curve

Fig. 12 shows the comparison between the simulation-based pressure prediction images and the experimental images. Four ROIs were chosen for comparison, and the average gray values were calculated. Consequently, the error was 5.46% without EM force, and it was 3.71% with EM force at 5 A. Even though these simulation results correspond well to the experiments, proficiency with the simulation software significantly affects the results, and it requires a relatively long computation time and cost. Therefore, we devised a CNN-based machine learning model using experimental data. Fig. 13 represents the generative image of the devised CNN model. The model requires three process conditions: the EM actuator air gap, current, and main force. The model is a type of decoder that receives three input values and expands them into images through three distinct kernels (30 × 30 → 10 × 10 → 3 × 3), which allows the model to construct the global pressure topology with the large kernel and gradually refine details with the smaller kernels.

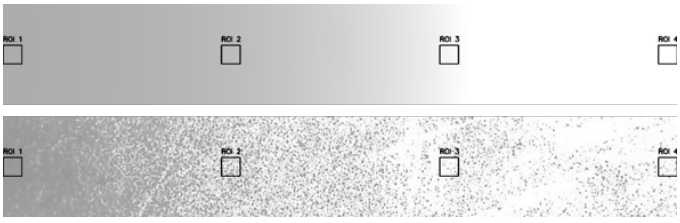


Figure 12 Simulation (Upper) vs Experiment (Lower)

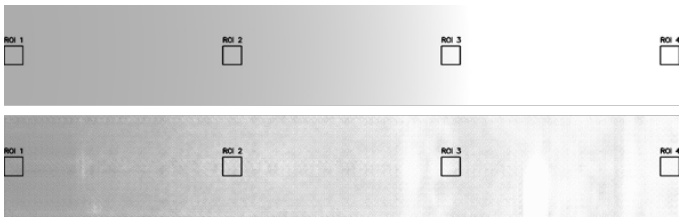


Figure 13 Simulation (Upper) vs CNN Image (Lower)

To evaluate the accuracy of the proposed model, the same comparison as the experiment and simulation cases was conducted. Four ROIs were chosen, and the average grayscale values were calculated. The results indicated that the errors were 4.92% without EM force and 6.04% with the 5 A EM force, respectively.

VI. Conclusion

This paper presented a lamination system that minimizes the pressure deviation, which can cause critical defects in large displays. As verified by the deviation ratio reduction with the auxiliary force, the proposed system can successfully be an alternative choice to the multiple-cylinder design that enlarges the entire system. In the simulation, the non-linear behavior of the electromagnetic actuator was confirmed, showing consistency with the experimental results. Furthermore, to substitute time-consuming simulation work and experiments, we devised a CNN-based machine learning model to predict surface pressure. This model showed errors of less than 7%, meaning that it can also be an efficient tool that does not require proficiency with simulation software.

Our future work will focus on developing a model that can be used for pressure prediction not only in the large-display lamination process but also in 3D lamination, such as for curved displays. Additionally, we used simple average gray values to compare the experimental and generative images, which is not sufficient to evaluate qualitative similarities. Therefore, we need to develop an appropriate evaluation method in the future.

Acknowledgment

References

[1] Ming, Wuyi, et al. "Progress in optical adhesive and lamination process of touch screen in 3C products." Journal of the Society for Information Display 30.12 (2022): 851-870

[2] Bahadur, Birendra, et al. “Direct dry film optical bonding – A low–cost, robust, and scalable display lamination technology.” Journal of the Society for Information Display 19.11 (2011): 732-740

[3] Oliveira, R., Viana, J., & Sampaio, P. (2023). Optical bonding process of flat panel displays and their critical-to-quality factors. The International Journal of Advanced Manufacturing Technology, 125(11), 5631-5650.

[4] Liggins, A. B., Stranart, J. C. E., Finlay, J. B., Rorabeck, C. H., & Little, E. G. (1992). Calibration and manipulation of data from Fuji pressure-sensitive film. Exp Mech, 1992, 61-70.

[5] SARAVANAN, Chandran. Color image to grayscale image conversion. In: 2010 second international conference on computer engineering and applications. IEEE, 2010. p. 196-199.

[6] Hutter, Kolumban, Alfons AF Ven, and Ana Ursescu. Electromagnetic field matter interactions in thermoelastic solids and viscous fluids. Springer, 2007.

[7] Lee, Eun-Ho. "A model for irreversible deformation phenomena driven by hydrostatic stress, deviatoric stress and an externally applied field." International journal of engineering science 169 (2021): 103573.

[8] Shim, Young-Dae, et al. "Integrated modeling framework for the interactions of plastic deformation, magnetic fields, and electrical circuits: Theory and applications to physics-informed real-time material monitoring." International Journal of Plasticity 184 (2025): 104212.